Available online at www.sciencedirect.com

ScienceDirect

IFAC PapersOnline CONFERENCE PAPER ARCHIVE

IFAC PapersOnLine 51-24 (2018) 620–627

An adaptive Extended Kalman Filter for monitoring and estimating key aircraft flight parameters

G. Alcalay*,*. C. Seren**. G. Hardier****
M. Delporte*. P. Goupil*

**AIRBUS Operations SAS, Toulouse, France (guillaume.alcalay@airbus.com)*
***ONERA – The French Aerospace Lab, Toulouse, France.*

Abstract: This paper addresses the selection and the monitoring of some key flight parameters along with their estimation in nominal and degraded flight conditions including faulty sensors situations. Anticipating more availability of flight parameters for future aircraft, isolating faulty measurements and reconstructing through time the missing signals is a challenging objective for Flight Control Systems, especially because some of them are essential for control purposes. To this end, this paper proposes a solution based on virtual sensors which make use of an Adaptive Extended Kalman Filter supplemented by dedicated Fault Detection and Isolation algorithm. It provides the ability for the longitudinal flight parameters of a civil aircraft to be estimated on-line before and after the occurrence of one or several failures. To facilitate onboard implementation, the main aerodynamic coefficients are approximated by a set of surrogate models. The proposed approach offers interesting monitoring capabilities including the detection of common mode failures (i.e., simultaneous failures occurring on redundant sensors). Real flight data involving strong atmospheric perturbations, 3-axis winds and successive faults on the static and total pressure probes from the take-off to the cruise is shown to evaluate the performances of the approach in terms of detection, isolation, estimation and reconfiguration capabilities

Keywords: Flight Control Systems, State estimation, Kalman filter, Fault detection, Virtual sensors

1. INTRODUCTION

The introduction of fly-by-wire in the early 80's increased the level of automation of civil aircraft (A/C) significantly, thanks to the development of advanced flight guidance and control laws. This major technological progress has also led to the development of new means for monitoring some key parameters and for protecting the flight envelop, hence improving the safety. This also provides tools to reduce the pilots' workload, which is especially valuable in case of unexpected situations. Actually, to keep a high level of automation available, some flight parameters such as the Angle of Attack (AoA/α) and the Calibrated Air Speed (CAS/V_C) are critical. Hence, their monitoring and robustness are major concerns, as well as extending their availability for use by the Flight Control Systems (FCS). They are usually measured by several sensors, but can also be computed onboard from other measurements. The classical solution relies on hardware redundancy so that some parameters are measured by several identical sensors. A majority-based voting mechanism is then used for Fault Detection and Isolation (FDI) in order to deliver so-called "consolidated" measurements, i.e. more accurate and fault tolerant measurements. A triplex voting scheme is used to cope with single failures, but, even if very improbable, simultaneous and consistent faults of two or three sources are difficult to detect. Besides, this solution penalizes the overall system performances in terms of weight, power consumption, space requirements, cost and extra maintenance needs. Solutions based on the principles of the so-called *analytical redundancy* can also achieve the objective of extending their availability without adding extra hardware complexity. Nevertheless, they require extended onboard computational capabilities, knowing they are still limited on current civil A/C.

Within the scope of estimation methods, model-based techniques have been investigated *(Marzat 2012, Seren 2013, Hardier 2013*). In this paper, we focus on nonlinear state estimators which permit residuals to be generated, that can be used for FDI purposes. Among them, recursive Bayesian filtering (*Deok-Jin 2005*) is well suited to deal with nonlinear systems. Under specific assumptions (*e.g.,* Gaussian stochastic uncertainties), it can provide a solution to the estimation problem while, in the general case, the exact analytical one is intractable in practice as it would require to calculate too complex multidimensional integrals. A first class of methods is related to analytical approximations in the Gaussian case and encompasses the well-known Extended Kalman Filter (EKF) (*Nørgaard 2000, Van Eykeren 2012, 2014, Seren 2013, Hardier 2015, Mohan 2015, Majumder 2016*). This one is still rarely implemented for A/C FDI with a notable exception of a recent application on board the latest A350 (*Lavigne 2011, Zolghadri 2015*). The EKF delivers an estimated state, recursively computed as a prediction (provided by an imperfect and uncertain model) corrected by an innovation term which makes use of noisy, but healthy, measurements. It permits to deal with both Gaussian distributions and system nonlinearities, the latter being usually linearized at the 1st-order. Since the approximations made in the EKF can sometimes lead to divergence and turn

2405-8963
Peer review under responsibility of International Federation of Automatic Control.
10.1016/j.ifacol.2018.09.640

out to be inappropriate for solving more complex and realistic problems, many other advanced techniques also exist. In theory, these techniques can manage system modeling uncertainties, unknown inputs, linearization errors, imperfect measurements, more complex noise distributions, and so on. Among others, sampling-based approaches such as Divided-Difference, Sigma-Point or Unscented Kalman Filters (*Chowdhary 2010, Marzat 2012, Van Eykeren 2012*) use a finite set of points, sampled in the state space, to describe the uncertainty distribution. These samples are then propagated through the nonlinear modeling in order to predict and update the *a posteriori* distribution. It can be proved that this results in a better approximation of the moments of the random distribution w.r.t. what is done in the EKF. Finally, a third category of techniques which seem to be efficient to deal with nonlinear and non-Gaussian filtering problems corresponds to direct numerical approximation observers or simulation-based filters, such as Finite-Difference, Sequential Monte-Carlo or Particle Filters (*Rawlings 2006*).

However, due to the stringent computational constraints for civil A/C, the most complex methods cannot be implemented onboard. Besides, A/C nonlinearities are not strong and do not require advanced algorithms to perform the estimation. Several studies (*Jazwinski 2007*) have demonstrated that analytical formulations using a 1st-order linearization can deal with A/C nonlinearities and measurement imperfections thanks to appropriate tuning. Hence an EKF-based algorithm is favored in this study, similar to the one developed in previous works (Seren 2013). Since sensor faults can occur during the flight, a self-adaptive method is also added to the estimation scheme. In the literature, several adaptive methods are proposed to deal with measurement uncertainties, making use of an adaptive tuning of the covariance matrices (Hide 2003). However, few solutions exist to face detected faulty and unavailable measurements over long time horizon. In this paper, an alternative solution is described. It relies on a new formulation of the filter equations, combined with an FDI algorithm which makes use of both the generated residuals and the estimated states. Compared to previous works (Seren 2015) that directly merge consolidated information, the proposed estimator makes only use of the measurements provided by the available anemometric sensors (pressure, temperature…). Moreover, complementary detection methods are also integrated into the scheme to isolate sensor faults. The remaining of the paper is organized as follows: section 2 presents the A/C modeling equations, and section 3 details the detection and adaptive algorithms. Finally, section 4 shows the performance and robustness of the overall estimation and detection scheme in realistic conditions corresponding to real flight test data with successive static and total pressure probes faults.

2. AIRCRAFT AND ATMOSPHERE MODELING

The proposed estimation scheme relies on a state space representation of a nonlinear A/C modeling, denoted by $\mathcal{M}_{NL}$ in what follows. It has been derived from both kinematic relationships and longitudinal flight mechanics s.t.:

$$\mathcal{M}_{NL}: \begin{cases} \dot{X} = f(X) + \xi_X \\ Y = h\big(X, Z, C_L(X,Z)\big) + \xi_Y \end{cases} \quad (1)$$

In (1), X (resp. Y) refers to the state (resp. output) vector. Z corresponds to a vector of reliable (*i.e.,* unfaulty) measurements required to compute the predicted output vector Y. It gathers the Euler angles (θ, φ, ψ), the pitch rate (q), the longitudinal load factor (n_X), the geopotential altitude (z_G) and the A/C ground speed components (V_{X0}, V_{Y0}, V_{Z0}) expressed in the reference Earth frame. C_L is a simplified model of the lift coefficient. As this model needs to be implemented onboard for computing the previous h function, an analytical surrogate modeling is used to replace the whole set of look-up tables required for updating the C_L value in terms of the actual flight parameters α, M (Mach number)... To build this surrogate modeling, a grey-box approach is favored to achieve a satisfactory trade-off between accuracy and complexity. The KOALA tool of the APRICOT modeling library is used (*Seren 2011, Biannic 2016*), part of the SMAC Toolbox (http://w3.onera.fr/smac/) developed by ONERA. Thanks to a special form of rational approximants (*Roos 2014*), the resulting surrogate C_L model can be easily implemented on-board, and facilitates the computation of the linearized expressions required by the EKF thanks to analytical derivations $(\partial h/\partial X)$. Finally, vectors ξ_X and ξ_Y of (1) are assumed to be process and observation Gaussian white noises, characterized by zero-mean, uncorrelated and mutually independent processes.

The most relevant flight parameters to describe the A/C behavior are the ones expressed w.r.t. the air mass flow. Many probes installed onboard provide a direct measurement of some air data parameters needed to control the aircraft. For instance, Pitot tubes, as well as both static pressure (P_s) and total air temperature (T_t) probes allow the CAS information to be computed onboard, as it is the most important velocity value for the FCS. Similarly, the redundant AoA probes provide direct measurements of this flight parameter, which is essential for both A/C flight envelop protection and autopilot. However, air data probes are subject to a harsh environment and failures can occur which require to reconfigure the FCS on the basis of the remaining valid sensors. Contrary to previous air data, inertial and A/C ground speed measurements, provided by Inertial Reference Systems (IRS) and the Global Positioning System (GPS) respectively, appear much more reliable and accurate since they take advantage of additional hardware redundancies and they are less sensitive to the environmental conditions. Besides, an onboard processing aims at consolidating these data. As a result, we consider in this paper that these data are trustworthy enough to focus on the estimation of the 3 wind speed components $\overrightarrow{W} = (W_{X0}, W_{Y0}, W_{Z0})$ (expressed in the reference Earth frame) and of some modeling errors (related to both aerodynamics and atmosphere). The choice of these states rather than the classical A/C ones for longitudinal flight parameters estimation allow limiting the complexity of the proposed estimator. All available anemometric measurements will be merged to reconstruct through time the critical longitudinal flight parameters (*i.e.,* AoA and CAS).

Therefore, the state vector X and process equations f are simply reduced to (omitting the state noise):

$$\dot{X} = \left(\dot{\vec{W}}, \dot{b}_{C_L}, \dot{\Delta}_{ISA}, \dot{z}_C\right) = f(X) = \left(\vec{0}, -b_{C_L}/\tau, 0, 0\right) \quad (2)$$

In (2), b_{C_L} refers to a bias on the aerodynamic lift force coefficient C_L to account for modeling uncertainty. Δ_{ISA} is the difference between the measured static temperature (denoted by T_s in the sequel) and the one given by the International Standard Atmosphere (ISA) reference modeling at the current geopotential altitude. z_C corresponds to a barometric correction term. The dynamics associated to the state variable components are modeled by both non-filtered and filtered random walks. For the state b_{C_L}, the time constant τ is set to several seconds. The physical meaning of the state variables Δ_{ISA} and z_C can be understood by analyzing the ISA modeling used for the computation of T_s and P_s (*ESDU 1986, 1992, 1996*). This model establishes both static temperature and pressure evolutions as a function of the altitude. Unfortunately, the resulting atmosphere description is not accurate enough. Some local effects, such as strong and inconsistent temperature and pressure gradients variations are not considered, introducing errors in the variables. One solution consists in re-estimating some of these errors (namely the 2 state components $(\hat{\Delta}_{ISA}, \hat{z}_C)$) to account for potential discrepancies. Thus, the ISA modeling states that:

$$\begin{aligned} &\text{if } z_G < z_{TP} \\ &\quad T_s = T_0 - G_Z z_G + \Delta_{ISA} \\ &\quad P_s = P_0(1 - G_Z z_P/T_0)^{g/(RG_Z)} \\ &\text{else} \\ &\quad T_s = T_{TP} + \Delta_{ISA} \\ &\quad P_s = P_{s_{TP}} \exp(-g(z_P - z_{TP})/(RT_0)) \end{aligned} \quad (3)$$

where $T_0 = 288.15$ K (resp. $P_0 = 101325$ Pa) and $T_{TP} = 216.65$ K (resp. $P_{s_{TP}} = 22632$ Pa) are the standard temperatures (resp. pressures) at ground and tropopause altitudes ($z_{TP} \approx 11$km) ; $G_Z = 6.5.10^{-3}$ K/m is the temperature gradient, g is the acceleration of gravity, $R = 287.053$ N.m/Kg.K is the specific gas constant for air. In (3), the altitude pressure z_P is calculated as follows:

$$\begin{aligned} &\text{if } z_G < z_{TP}, \quad z_P = z_G/(1 + \Delta_{ISA}/T_0) - z_C \\ &\text{else} \qquad\quad z_P = z_G/(1 + \Delta_{ISA}/T_{TP}) - z_C \end{aligned} \quad (4)$$

i.e., is directly deduced from the measured geopotential altitude z_g and the predicted state Δ_{ISA} (*ESDU 1986, 1992, 1996).* This result is then corrected by the z_C term, as depicted on Figure 1.

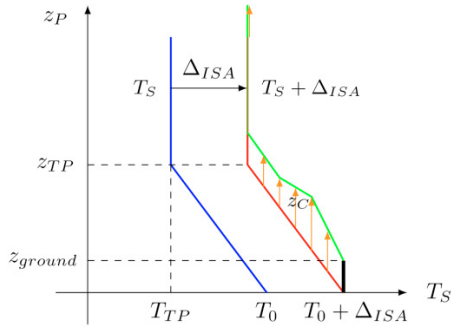

Fig. 1. (Δ_{ISA}, z_c) representation and the ISA modeling

The measurements used for data fusion include the AoA and the sideslip (β) angle, the vertical load factor (n_Z), both static (P_s) and total (P_t) pressures (from the Pitot tubes), and the total air temperature (T_t). Besides, it is noteworthy that some additional information coming from the engine nacelle permits 2 extra pseudo-measurements of the static pressure (denoted by P_s^{eng}) and of the Mach number (M^{eng}) to be reconstructed. This also provides a direct, and hence redundant, measurement of the total air temperature denoted by T_t^{eng}. However, all this redundant information is not used for state and output estimation but only for FDI. The whole set of measured data provide enough information for the observability condition to be held. The observation equations denoted by h read:

$$h(X,Z) = \begin{pmatrix} \alpha = \text{atan}(w/u) \\ \beta = \text{atan}(v/\sqrt{u^2 + w^2}) \\ n_Z = \dfrac{\gamma S P_s M^2 \left(C_L + b_{C_L}\right)}{2mg\cos\alpha} + n_x \tan\alpha \\ P_s = \mathcal{F}(z_P(z_G, z_C), \Delta_{ISA}) \\ P_t = P_s(1 + \bar{\gamma}M^2)^{\gamma/(\gamma-1)} \\ T_t = T_s(1 + \bar{\gamma}M^2) \end{pmatrix} \quad (5)$$

where $\gamma = 1.4$, $\bar{\gamma} = (\gamma - 1)/2$, S is the A/C reference surface, m its weight, and C_L depends on X and Z. Once an anemometric measurement (P_s, P_t or T_t) becomes faulty and is isolated thanks to a simple FDI logic (*Alcalay 2017*), the estimation scheme is updated to make use of the engine measurements ($P_{t_{eng}} = \mathcal{G}(P_{s_{eng}}, M_{eng})$, $P_{s_{eng}}, T_{t_{eng}}$) instead. In (5), the dependency of the static pressure P_s w.r.t. z_G, z_C and Δ_{ISA} reveals that this output is actually calculated by using (3) with the corrected altitude pressure z_P drawn from (4). (u, v, w) are the airspeed components expressed in the reference body frame. They are deduced from (6) where $R(\theta, \varphi, \psi)$ represents the usual rotation matrix from the reference Earth frame to the A/C body one:

$$\begin{pmatrix} u \\ v \\ w \end{pmatrix} = R(\theta, \varphi, \psi) \cdot \begin{pmatrix} V_{X0} - W_{X0} \\ V_{Y0} - W_{Y0} \\ V_{Z0} - W_{Z0} \end{pmatrix} \quad (6)$$

Then, the Mach number M is computed s.t.:

$$M = V/\sqrt{\gamma R T_s} = \sqrt{u^2 + v^2 + w^2}/\sqrt{\gamma R T_s} \quad (7)$$

Finally, the CAS value is determined according to the following expression (*ESDU 1992*):

$$V_C = \sqrt{\frac{\gamma R T_0}{\bar{\gamma}}} \left(\left(1 + \frac{P_t - P_s}{P_0}\right)^{(\gamma-1)/\gamma} - 1 \right)^{0.5} \quad (8)$$

Thanks to model equations (2)-(8) and available measurement data, the key flight parameters (α, V_C) can be estimated through time, while the FDI algorithm detailed in (*Alcalay 2017*) and section 3 monitors the possibly faulty information. In case of sensor failures or erroneous weight data capture by the pilot (*Alcalay 2017*), a reconfiguration of

the estimation scheme is required in order to deliver reliable estimates $(\hat{\alpha}, \hat{V}_C)$ continuously. Moreover, it has to be noticed that the linearized matrices $(\partial f/\partial X, \partial h/\partial X)$ required in the standard EKF algorithm can be easily computed analytically in our case. Indeed, the main computational effort lies in the derivation of the $\partial C_L/\partial X$ term, for which an analytical expression can be obtained thanks to the use of surrogate models. This significantly reduces both the computational time and the complexity of the proposed method. A sequential processing of the measurements during the correction stage has also been implemented to avoid any matrix inversion (*Zhou 2010*) whose complexity is not compliant with the available embedded CPU on Airbus A/C. Beyond its computational efficiency, this procedure permits also any detected faulty measurements to be skipped very easily.

The next section describes the FDI algorithm which has been developed to confer a self-adaptive capability on the proposed estimation scheme in case of sensor faults. The ultimate goal is to deliver reliable estimates $(\hat{\alpha}, \hat{V}_C)$ for the rest of the flight, even in faulty situations.

3. MONITORING AND FAULT DETECTION

The proposed EKF-based estimation scheme acts as a virtual clinometric and anemometric sensor by providing dissimilar AoA and CAS information. However, any EKF needs healthy measurements as inputs to work properly. Consequently, if a fault occurs on one or several measurements used for data fusion, a reconfiguration is required to prevent them from degrading the estimation process. This permits reliable flight parameter estimates to be provided to the FCS, namely AoA and CAS, even in degraded situations when sensor faults occur. Hence, an efficient and fast detection and isolation of the fault is mandatory. The inertial and A/C ground speed measurements, provided by the IRS and GPS, are already monitored by several dedicated systems, as explained in section 2, and only the faults on the AoA, P_t, P_s and T_t probes are considered in the sequel.

3.1. An EKF-based fault detection procedure

To perform the detection, the EKF delivers some crucial information through the modeling bias estimate $\hat{b}_{C_L}$. In case of faulty AoA, P_t, P_s probes, the existing relation between the flight parameters through the vertical load factor output equation (5) and the computed lift force coefficient $C_L(X,Z)$ affects $\hat{b}_{C_L}$ during the transient stage, when the fault is not yet isolated and the filter not reconfigured. This is a direct consequence of the EKF tuning, leading the estimated state $\hat{b}_{C_L}$ to be sensitive to several disturbances such as sensor delays, biases and failures. However, this has two advantages. Firstly, an adaptive threshold J_{C_L} can be tuned to detect the occurrence of some faults, as depicted in Figure 2. It shows the evolution of the modeling bias depending on the Mach number and the A/C aerodynamic configuration (*i.e.,* slats/flaps positions) after a take-off. A Monte Carlo validation has been performed on real flight data to define this threshold regarding the modeling accuracy and the flight conditions. Several realistic defects such as small delays or biases on the measurements, as well as small weight errors, have been simulated and added to the flight data during the validation process. Secondly, the type of fault occurring is identified through a pseudo-derivative filter applied to $\hat{b}_{C_L}$. The resulting slope and its dynamics is used as a global indicator of the fault type. This characterization stage is particularly important to detect slow drifts since they cannot be isolated by the scheme as presented further in 3.3. Consequently, a dedicated indicator I_{SL} is computed to point out that an unidentified fault has occurred ($I_{SL} = 1$), as depicted in Figure 2. The other elements of this figure are explained further in this section.

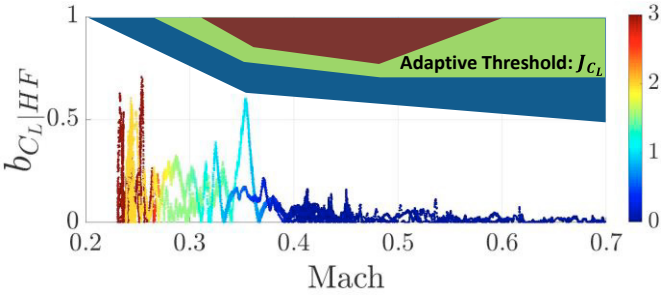

*Fig. **2**. High frequency normalized $\mathbf{b_{C_L}}$ function of the Mach number and the A/C aerodynamic configuration with its related adaptive threshold*

3.2. Standard isolation based on dissimilar equation errors

A usual approach to perform the isolation procedure is to use redundant measurement data by comparing them two by two in order to isolate the faulty information. Considering the four parameters to be monitored (AoA, P_t, P_s and T_t), three dissimilar values of M squared can be derived from equation (5):

$$M_P^2 = 1/\bar{\gamma}\left[\left(P_{t_m}/P_{S_m}\right)^{(\gamma-1)/\gamma} - 1\right] \quad (9.1)$$

$$M_T^2 = 1/\bar{\gamma}\left(T_{t_m}/T_S - 1\right) \quad (9.2)$$

$$M_L^2 = 2mg\cos\alpha_m\left(n_Z - n_X\tan\alpha_m\right)/\left(\gamma S P_{S_m} C_L(\alpha_m, \ldots)\right) \quad (9.3)$$

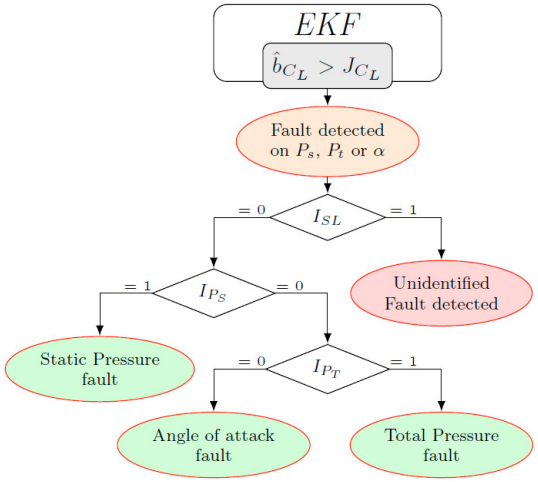

*Fig. **3**. FDI decision scheme*

where the subscript m refers to measurement values. T_s is the static temperature computed from (3) with Δ_{ISA} and z_c values fixed at previous estimated values provided by the EKF in healthy conditions. C_L is the lift force coefficient computed by the surrogate model with measured flight parameters as inputs. From (9), three residuals can be derived:

$$\begin{aligned} \varepsilon_{PT} &= M_P^2 - M_T^2 \\ \varepsilon_{PL} &= M_P^2 - M_L^2 \\ \varepsilon_{TL} &= M_T^2 - M_L^2 \end{aligned} \quad (10)$$

Each of them can be associated to a corresponding threshold, denoted by J_{PT}, J_{PL} and J_{TL} respectively. From (9)-(10), a single common mode failure (for instance simultaneous and coherent failures occurring on the AoA probes) would impact several residuals and the isolation would be performed thanks to the logical Table 1.

Table 1: Fault signatures on residuals

	$\epsilon_{PT} > J_{PT}$	$\epsilon_{PL} > J_{PL}$	$\epsilon_{TL} > J_{TL}$
P_t	Yes	Yes	No
P_S	Yes	Yes	Yes
α	No	Yes	Yes
P_S *or* T_t	Yes	No	Yes

Table 1 means that, for instance, once J_{PL} and J_{TL} are exceeded by their corresponding residual, a fault can be identified on the AoA measurement. This comes from the fact that the Mach number computed from (9.3) is erroneous, due to the injection of faulty AoA values in its computation. On the contrary, the Mach numbers from both (9.1) and (9.2) are still consistent since the P_t, P_s and T_t measurements are valid. Consequently, the computed residual ϵ_{PT} is not going to exceed its threshold J_{PT}. However, the solution described yields good results with simulated data but when applied to real flight data, even with perfectly tuned thresholds, the local atmospheric fluctuations on Δ_{ISA} and z_C raise too many false alarms and result in poor isolation performances. Besides, performing the distinction between two or three exceeded thresholds (to distinguish a fault between the static pressure and the other measurements) is almost impossible in strong atmospheric fluctuation.

3.3 A signal-based isolation approach

An alternative solution for the isolation procedure is to take advantage of simple signal processing methods, such as filtering operations and signal comparisons. First, a dedicated monitoring on the T_t is possible, by comparing its value with the one delivered by the engine temperature sensor. In addition, two new indicators are introduced in the subsection *3.3* to perform the isolation between a fault on the AoA, P_t and P_s probes. They are derived from specific signals chosen for their dependency to a maximum of 2 among the 3 parameters.

In order to perform the distinction of a fault between the AoA and the pressure measurements (P_t, P_s), a first monitoring signal is based on the variation of the computed Mach number using (9.1) depending on the pressure measurements. Any variation on the Mach number can result from pilot orders or atmospheric parameter variations, especially the wind. Hence, a high pass filter is applied to the signal with a cut-off frequency beyond the ones associated to the typical A/C dynamics. The resulting signal includes high frequency (HF defined as the frequencies beyond the usual A/C bandwidth) local atmospheric variations and wind gradients as well as potential faults. Figure 4 shows that the resulting signal variations in nominal conditions mainly depends on two parameters: 1/ the ground speed module variation ΔV_g, reflecting the remaining medium-high frequency pilot orders; 2/ the ground speed vertical component V_{g_z}, reflecting the flight level variations and so the possible resulting HF variation in the atmospheric parameters. Figure 4 illustrates the effects of these two parameters on the HF Mach variations, using 20 hours' flight records, through a scatter plot where the color of each point is related to its corresponding V_{g_z} value. As depicted in Figure 4, an adaptive threshold can be defined depending on those two parameters. Once exceeded, the unusual event can be interpreted as a fault on one of the pressure sensors used to compute the Mach number. Consequently, a first indicator (denoted I_{PT} in Figure 3) is defined, pointing the suspicious probes out between the AoA and pressures measurements.

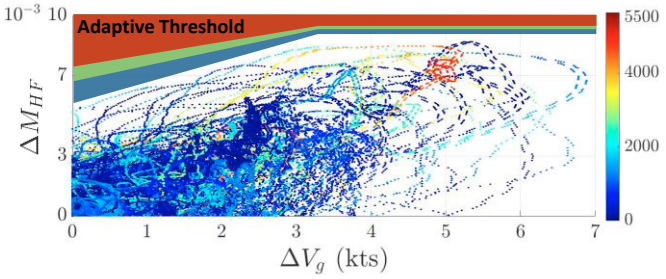

Fig. **4**. $\Delta M_{HF} = f(\Delta V_g, V_{g_z})$ *and its related adaptive threshold on 20h flight records*

A second indicator I_{PS} can be derived with the same approach, to help make a decision between a fault on the static pressure and the other sensors. (3) gives a direct relation between the P_s measurement and the pressure altitude z_p. Besides, (4) links the geometric altitude z_G with z_P thanks to the atmospheric parameters, essentially characterized by low frequency variations at a constant flight level with possible abrupt changes with altitude variations. In order to isolate a fault on the static pressure probes, we choose to monitor the HF component of $z_P - z_G$.

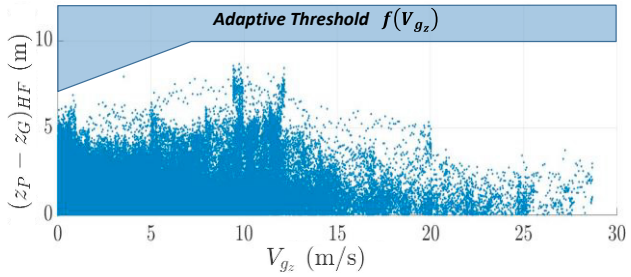

Fig. **5**. $(z_P - z_G)_{HF} = f(V_{g_z})$ *and its related adaptive threshold on 20h flight records*

Figure 5 shows on 20 flight hours that this HF difference is restricted and that the highest values are related to important or medium V_{g_z} values. Hence a monitoring is possible using an adaptive threshold depending this time only on V_{g_z}, and the same conclusion can be made as for I_{PT} when the threshold is exceeded. However, the relation monitored in this case leads to isolate the fault on the P_S measurement.

To sum up, these two monitoring schemes permit unusual variations of P_t and P_s measurements to be identified, which are very likely to be sensor faults. Coupled with the results of the EKF-based detection and fault characterization (through the lift force equation consistency check), it permit to decide if this unusual variation corresponds to strong atmospheric turbulences or a fault. Finally, a complete and efficient FDI algorithm is achieved. As depicted in Figure 3, the limitation induced by the use of several high pass filters leads some low frequency faults to be detected while remaining unidentified. These faults are typically slow drift errors on the sensors. The performance of the EKF coupled with this FDI algorithm is depicted on Figures 6 - 7. They represent the maximum estimation error on the AoA and CAS parameters in case of isolated sensor faults (drifts, biases, …) depending on the Mach number and the A/C configuration, through Monte Carlo simulations using real flight data and simulated faults. λ_{CAS} and λ_α denote the maximum errors targeted.

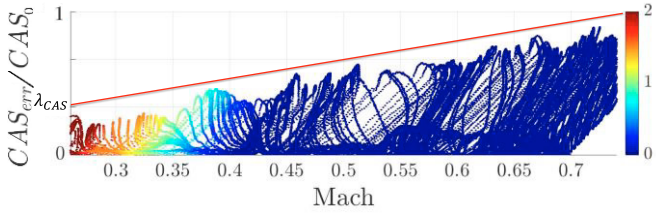

Fig. **6**. *Normalized maximum* CAS *errors function of the Mach number and the A/C aerodynamic configuration*

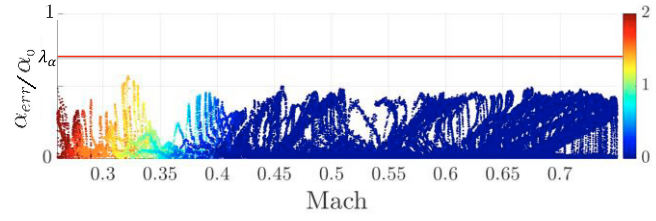

Fig. **7**. *Normalized maximum AoA errors function of the Mach number and the A/C aerodynamic configuration*

4. RESULTS

The proposed Adaptive Extended Kalman Filter (AEKF) was evaluated from multiple simulations (using the high fidelity AIRBUS tool) and real intercontinental flight test data coming from a generic civil transport A/C, including atmosphere disturbances, strong winds, and variations of both temperature and pressure gradients. The results displayed in section 4 are obtained after post-processing the real data recorded during a flight between Iqaluit (Canada) and Toulouse (France). These data span the first 50 minutes of the flight, starting from the take-off until the beginning of the cruise phase. An analysis of the data has shown that, during the climb phase, the airplane came across a Δ_{ISA} around 40 K, a z_C greater than 900 m and a 3-axis wind with wind speed values up to 30 kts. The time history of these variables is plotted in Figures 8 - 9.

In order to evaluate the whole process, simulated sensor faults have been added to the real flight data. Accordingly,

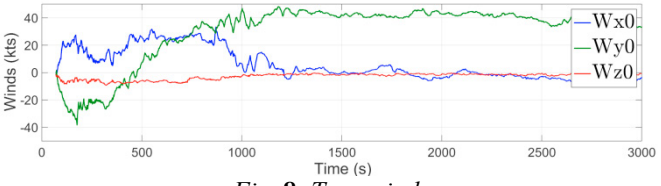

Fig. **8**. *True winds*

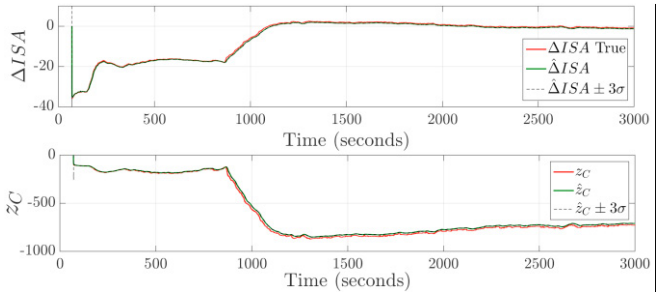

Fig. **9**.*True* Δ_{ISA} *&* $\mathrm{z_c}$

the full scenario is the following: the take-off is at $t = 80s$, a common drift (slope 60mbar/s) is superimposed to the Ps probes #1 and #2 at $t = 115s$, then a drift (100mbar/s) on the P_t probes is generated at $t = 250s$. At $t = 2115s$, the P_t measurement is available again with a small bias. It is worth noting that a triplex-based voting mechanism is used onboard to deliver consolidated measurements. Hence, for each measured parameter, 3 probes are respectively available and should be monitored by the FDI scheme. This makes sure that any valid information is used to feed the EKF, as it would be the case in this example for the P_s probes #3.

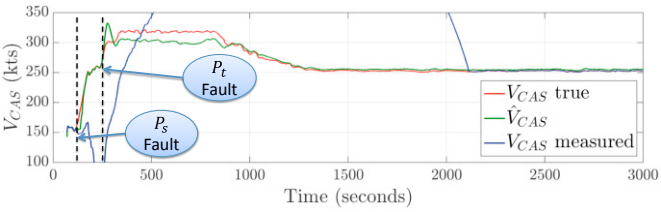

Fig. **10**. *CAS estimated, true and measured in case of multiple pressure sensor faults*

Figure 10 compares the time history of the estimated CAS (green line) with those of the CAS measurements (blue line) computed from P_t and P_s measurements and with the true CAS (red line). Several reconfigurations are performed throughout this scenario. They consist in selecting which among the triplex sensors are still unfaulty, by relying on a direct comparison of the 3 measured values with the estimated one. The scenario illustrates the capability of the proposed approach for 1/ detecting and isolating sensors faults, 2/ delivering reliable estimates over a long time horizon despite degraded flight conditions.

The time variation of the normalized $\hat{b}_{C_L}$ is plotted in Figure 11, with the associated thresholds (dashed red lines). It can be noticed that $\hat{b}_{C_L}$ is sensitive to all sensors faults (regardless of

their type). Lower and upper threshold adaptations with the flight point can also be observed on this plot.

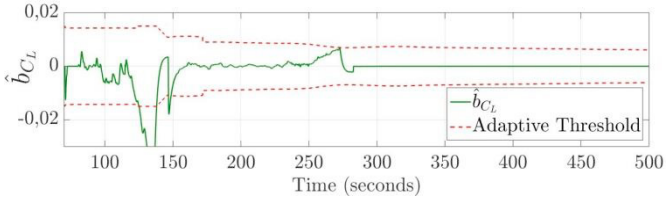

Fig. **11**. *Estimated* $\hat{b}_{C_L}$ *in case of multiple pressure sensor faults*

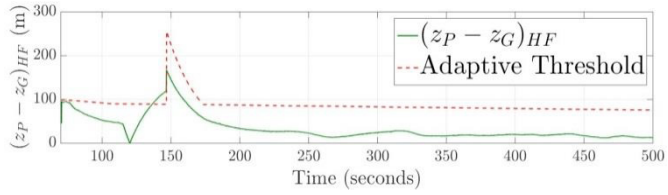

Fig. **12**. $(z_P - z_G)_{HF}$ *generated to compute* I_{P_S}

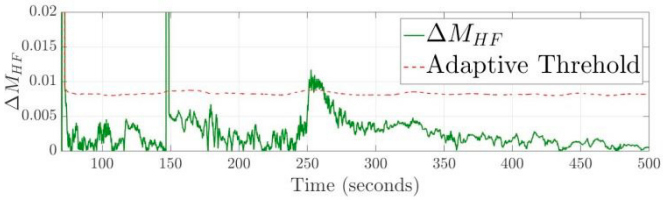

Fig. **13**. ΔM_{HF} *generated to compute* I_{P_t}

Figures 12 and 13 show the evolution during the first 500 seconds of the HF signals generated to compute the values of the two indicators I_{P_T} and I_{P_S}. The successive pressure sensor faults are detected once their corresponding errors are significant enough. Regarding the CAS parameter, the detection performances are linked to the flight phase. Once the error is between 15kts and 50kts, depending on the flight phase, a fault is detected, the isolation is performed and the missing flight parameters are estimated. In this example, the P_s drift fault is detected and isolated at $t = 135s$ ($I_{SL} = 0$, $I_{P_T} = 0$ and $I_{P_S} = 1$). Then, the filter is firstly reconfigured by removing the faulty P_S measurements. An estimation of its value is performed up to $t = 150s$, when the P_s measurement delivered by probe #3 is declared healthy. As a result, the filter is again reconfigured to use the valid remaining P_S information and the FDI scheme is deactivated briefly while the filter is converging (< 5s). This evaluation proves that a so-called common mode failure can be properly detected and isolated by the proposed scheme. Then, the drift on the P_t probes are detected at $t = 272s$ ($I_{SL} = 0$, $I_{P_T} = 1$ and $I_{P_S} = 0$) and the three probes are rejected up to their validation around $t = 2120s$. Between those time instants, $\hat{b}_{C_L}$ is no longer estimated (figure 11) hence $\hat{P}_t$ strongly depends on the internal model which also results from a trade-off between the model accuracy and the implementation constraints. Nevertheless, the estimated flight parameters appear accurate enough to be used as inputs for the FCS during the remaining part of the flight.

5. CONCLUSIONS

The proposed AEKF algorithm offers some very interesting capabilities to detect sensor faults and to estimate key longitudinal flight parameters in degraded conditions with a limited complexity. The approach is based on an original formulation including states such as wind components, atmospheric perturbations, and some modeling biases. Besides, the algorithm combines simple signal processing methods with the estimated states of the EKF to perform the fault isolation. Finally, the performances are closely linked to the estimator model accuracy, only involving the lift force coefficient. That is why a surrogate model was developed to fit the onboard computational constraints while keeping a satisfying accuracy. Nevertheless, some prospects arise from the present choice of introducing a barometric correction term zc, which absorbs additional atmospheric effects such as the temperature gradient fluctuation, hence loosing part of its real physical meaning. Instead, an additional module could be used to estimate the temperature gradient and to remove its effect from zc. The current choice has been made to minimize the number of states, and consequently the computation burden of the algorithm.

REFERENCES

Alcalay, G., Seren, C., Hardier, G., Delporte, M., Goupil, P. (2017) Development of virtual sensors to estimate critical aircraft flight parameters, IFAC World Congress, Vol. 50(1), pp.14174-14179.

Biannic, J.M., *et al.* (2016) Surrogate models for aircraft flight control: some off-line and embedded applications. *AerospaceLab Journal*, Issue (12), (http://www.aerospacelab-journal.org/al12), pp. 1-21.

Chowdhary, G., Jategaonkar, R. (2010) Aerodynamic parameter estimation from flight data applying extended and unscented Kalman filter. *Aerospace Science and Technology*, Vol. 14(2), pp. 106-117.

Deok-Jin, L. (2005) Nonlinear Bayesian filtering with applications to estimation and navigation. *PhD Thesis* – Texas A&M University.

ESDU (1986) Equations for calculation of International Standard Atmosphere and associated off-standard atmospheres. *ESDU Item No.77022 (Amendments A, B)*.

ESDU (1992) Airspeed data for performance calculations. *ESDU Item No.69026 (Amendment B, October 1992)*.

ESDU (1996) Height relationships for non-standard atmospheres. *ESDU Item No.78012 (Amendment B, November 1996)*.

Hardier, G., Seren, C., Ezerzere, P., Puyou, G. (2013) Aerodynamic model inversion for virtual sensing of longitudinal flight parameters. *2nd IEEE SysTol Conf.*, Nice, France, pp. 25-30.

Hardier, G., Seren, C., Ezerzere, P. (2015) Model-based techniques for virtual sensing of longitudinal flight parameters. *Intal Journal of Applied Mathematics and Computer Science*, Vol. 25(1), pp. 23-38.

Hide, C., Moore, T., Smith, M. (2003) Adaptive Kalman filtering for low-cost INS/GPS. *The Journal of Navigation*, Vol. 56(1), pp. 143-152.

Jazwinski, A.H. (2007) Stochastic processes and filtering theory. *Courier Corporation*.

Lavigne, L., Zolghadri, A., Goupil, P., Simon, P. (2011) A model-based technique for early and robust detection of oscillatory failure case in A380 actuators. *Int^al Journal of Control, Automation and Systems*, Vol. 9(1), pp. 42-49.

Majumder, R., Sadhu, S. (2016) Robust extended Kalman filter for ballistic object tracking during re-entry. *IEEE annual INDICON Conf.*, pp. 1-6.

Marzat, J., Piet-Lahanier, H., Damongeot, F., Walter, E. (2012). Model-based fault diagnosis for aerospace systems: a survey. *Journal of Aerospace Engineering*, Vol. 226(10), 1329-1360.

Mohan, *et al.* (2015) Introduction to the Kalman filter and tuning its statistics for near optimal estimates and Cramer-Rao bound. *Technical Report TR/EE2015/401, Department of Electrical Engineering, Indian Institute of Technology*, Kanpur.

Nørgaard, M., Poulsen, N. K., Ravn, O. (2000) New developments in state estimation for nonlinear systems. *Automatica*, Vol. 36(11), pp. 1627-1638.

Rawlings, J. B., Bakshi, B. R. (2006) Particle filtering and moving horizon estimation. *Computer & Chemical Engineering*, Vol. 30(10–12), pp. 1529-1541.

Roos, C., Hardier, G., Biannic, J-M. (2014) Polynomial and rational approximation with the APRICOT library of the SMAC toolbox. *IEEE Multiconference on Systems and Control*, Antibes, France, pp. 1473-1478.

Seren, C., Hardier, G., Ezerzere, P. (2011) On-line estimation of longitudinal flight parameters. *SAE AeroTech Congress and Exhibition*, Toulouse, France.

Seren, C., Hardier, G., Ezerzere, P., Puyou, G. (2013) Adaptive extended Kalman filtering for virtual sensing of longitudinal flight parameters. *2^nd IEEE SysTol Conf.*, Nice, France, pp. 25-30.

Van Eykeren, L., Chu, Q. P., Mulder, J. A. (2012) Sensor fault detection and isolation using adaptive extended Kalman filter. *8^th IFAC SafeProcess Conf.*, Vol. 45(20), pp. 1155-1160.

Van Eykeren, L., Chu, Q. P. (2014) Sensor fault detection and isolation for aircraft control systems by kinematics relations. *Control Engineering Practice*, Vol. 31, pp. 200-210.

Zhou, J., Knedlik, S., Loffeld, O. (2010) Sequential processing of integrated measurements in tighly-coupled INS/GPS integrated navigation system. *AIAA Conf. on GNC*, Toronto, Canada, pp. 2-5.

Zolghadri, A., *et al.* (2015) Signal and model-based fault detection for aircraft systems. *9^th IFAC SafeProcess Conf.,* Vol. 48(21), pp. 1096-1101, Paris, France.